Anatomizing the Ocean's Role in ENSO Changes under Global Warming*

HAIJUN YANG+

Department of Atmospheric Science, School of Physics, Peking University, Beijing, China

QIONG ZHANG+

State Key Laboratory of Numerical Modeling for Atmospheric Sciences and Geophysical Fluid Dynamics, Institute of Atmospheric Physics, Chinese Academy of Sciences, Beijing, China

(Manuscript received 9 November 2007, in final form 30 May 2008)

ABSTRACT

A revisit on observations shows that the tropical El Niño–Southern Oscillation (ENSO) variability, after removing both the long-term trend and decadal variation of the background climate, has been enhanced by as much as 50% during the past 50 yr. This is inconsistent with the changes in the equatorial atmosphere, which shows a slowdown of the zonal Walker circulation and tends to stabilize the tropical coupling system. The ocean role is highlighted in this paper. The enhanced ENSO variability is attributed to the strengthened equatorial thermocline that acts as a destabilizing factor of the tropical coupling system. To quantify the dynamic effect of the ocean on the ENSO variability under the global warming, ensemble experiments are performed using a coupled climate model [Fast Ocean Atmosphere Model (FOAM)], following the "1pctto2x" scenario defined in the Intergovernmental Panel on Climate Change (IPCC) reports. Term balance analyses on the temperature variability equation show that the anomalous upwelling of the mean vertical temperature gradient (referred as the "local term") in the eastern equatorial Pacific is the most important destabilizing factor to the temperature variabilities. The magnitude of local term and its change are controlled by its two components: the mean vertical temperature gradient $\overline{T}_z$ and the "virtual vertical heat flux" $-w'T'$. The former can be viewed as the background of the latter and these two components are positively correlated. A stronger $\overline{T}_z$ is usually associated with a bigger upward heat flux $-w'T'$, which implies a bigger impact of thermocline depth variations on SST. The $\overline{T}_z$ is first enhanced during the transient stage of the global warming with a 1% yr^{-1} increase of CO_2, and then reduced during the equilibrium stage with a fixed doubled CO_2. This turnaround in $\overline{T}_z$ determines the turnaround of ENSO variability in the entire global warming period.

1. Introduction

El Niño–Southern Oscillation (ENSO) is the leading mode of atmosphere–ocean coupled variability on interannual time scales in the tropical Pacific and can affect global climate substantially. The change in ENSO properties due to background climate shift is the subject of much debate. Some paleoclimatic studies reveal that ENSO has undergone significant climate shifts in the history in response to a background climate change (Liu et al. 2000; Cole 2001; Tudhope et al. 2001; Rosenthal and Broccoli 2004). Some studies on the high-resolution fossil–coral record, however, suggest a poor relationship between the ENSO activity and the mean climate during the last millennium, and the ENSO behavior has a broad range that may arise from dynamics internal to the ENSO system itself (Cobb et al. 2003). There are great uncertainties concerning the relationship between ENSO characteristics and the background climate state.

Studies on the past century's observations suggest that judging whether the ENSO is shifting or not could be contingent on how we view the background climate.

* Peking University School of Physics Department of Atmospheric Science Contribution Number 005.

+ Current affiliation: Bert Bolin Centre for Climate Research, and Department of Meteorology, Stockholm University, Stockholm, Sweden.

Corresponding author address: Haijun Yang, Department of Atmospheric Science, School of Physics, Peking University, 209 Chengfu Road, Beijing 100871, China.
E-mail: hjyang@pku.edu.cn

DOI: 10.1175/2008JCLI2324.1

The tendency for more El Niño and fewer La Niña events is clear since the late 1970s if the background climate is viewed as constant (Trenberth and Hoar 1996). When considering the decadal change of the tropical Pacific background climate, the El Niño and La Niña still occur alternatively and their amplitudes are comparable (Fedorov and Philander 2000). These raise concerns on the uncertainty of assessing the ENSO properties in a future climate.

ENSO might be subject to change in the future as a result of anthropogenic warming. Recently, the ENSO behaviors in an enhanced greenhouse gases (GHGs) scenario of phase 3 of the Coupled Model Intercomparison Project (CMIP3) coupled models evaluated for the Fourth Assessment Report (AR4) of the Intergovernmental Panel on Climate Change (IPCC; additional information is available online at http://www-pcmdi.llnl.gov/ipcc/about_ipcc.php) have been examined extensively (An et al. 2008; Philip and van Oldenborgh 2006; Guilyardi 2006; Merryfield 2006; van Oldenborgh et al. 2005; Meehl et al. 2006). Considerable studies suggest that although it would cause significant changes in global mean climate, the future global warming has little impact on the ENSO properties (Philip and van Oldenborgh 2006; Guilyardi 2006; van Oldenborgh et al. 2005; Zelle et al. 2005) because the destabilizing and stabilizing factors of the atmosphere and ocean compensate each other. Some studies show that the significance of the ENSO amplitude reduction in CO_2 increasing experiments depends on the extent of the change in the mean state or the strength of the external forcing (Meehl et al. 2006). The most recent analysis on CMIP3/IPCC AR4 coupled model outputs by An et al. (2008) shows a multidecadal modulation of ENSO in response to increasing GHGs. The latter is related to the delayed response of the subsurface temperature in the tropical Pacific compared to the response time of the sea surface temperature (SST). They further suggest that the delayed response of the subsurface temperature can lead a modulation of the vertical temperature gradient in the tropical Pacific, which is a crucial mechanism to understand the transient behavior of the ENSO variability in the global warming.

Because of the high diversity of the predicted ENSO sensitivity to the future warming by coupled models, a revisit on observations is quite necessary. A reexamination of the past ocean temperature observations in this work suggests that the ENSO variability has been enhanced by as much as 50% during the past 50 yr. We emphasize that this is obtained by removing both the long-term trend and decadal variations of the background climate. The ENSO amplitude change under this circumstance has not been paid sufficient attention in previous studies. The enhanced ENSO amplitude can be attributed to the strengthened thermocline in the equatorial Pacific, which plays as a destabilizing effect on the tropical coupling system (An et al. 2008). However, the observations also show that the tropical atmosphere becomes more stable because of the slowdown of the zonal Walker circulation (Vecchi et al. 2006; Vecchi and Soden 2007). This tends to stabilize the tropical coupled variability. The enhanced ENSO variability in observations suggests that the stabilizing factors of atmosphere cannot compensate the destabilizing factors of the ocean as implied by many coupled models. The ocean appears to play a more important role. This motivates us to scrutinize the ocean roles in the global warming.

The warming in the world climate can be divided into two stages: the transient stage and the equilibrium stage. In the transient stage the atmosphere adjusts quickly to the varying external forcings so that it is always in a dynamic equilibrium state under the global warming. The ocean, however, experiences changes that mainly concentrate near the surface because of its large thermal inertia. In the equilibrium stage with fixed external forcings, the atmosphere is almost constant while the ocean is still evolving, which would persist for a considerable time because of the slow downward penetration of the surface changes. The ocean may play very different roles in these two stages and affect coupled climate variabilities differently because of the delayed response of the subsurface ocean, particularly for the equatorial ocean where the thermocline dynamics are vital to the surface climate. Of course this division on the global warming is based on the assumption that the GHGs would not increase unlimitedly, similar to the "1pctto2x" scenario defined in the IPCC reports.

The ocean roles in different stages of the global warming are anatomized using the method of term balance analyses in this paper, with focus on the ocean roles only in the ENSO variability. Different from previously qualitative analyses on the effect of the equatorial thermocline by sensitivity experiments of coupled models, the dynamic effects of the equatorial stratification on the ENSO strength are quantified through the term balance analyses on the derived temperature variability equation. The enhanced ENSO variabilities in the past 50 yr as well as in the transient stage of the global warming result from the enhanced equatorial stratification. The latter occurs because the subsurface ocean needs a much longer time than the surface ocean to warm up (An et al. 2008). However, once the ocean at depth reaches the equilibrium, the ENSO variability would have to reduce in response to the weakened

equatorial stratification in the equilibrium stage. We conclude in this paper that the turnaround in the strength of the equatorial stratification controls the turnaround in the ENSO variability. In this sense, this study is consistent with other coupled models' predictions of a weaker ENSO in a future warmed climate (e.g., Meehl et al. 2006).

The dynamic effects of the atmosphere on the ENSO variability are also carefully examined in this work. The weakened mean trade winds in the global warming can lead to a more stable equatorial atmosphere. The term balance analyses disclose that the suppression of air–sea coupling in a stable atmosphere is not merely attributed to the weakened mean upwelling but, more important, the enhanced vertical gradient of temperature variabilities under the background of weakened mean upwelling. More specifically, the weakened mean upwelling in the Niño-3 region will hinder the interaction between the thermocline and the surface, or in other words, reduce the impact of the thermocline variability on the surface variability. The dynamic connection between a weakened trade wind and a weak air–sea interaction is then established.

This paper focuses on the changes in the climate variability, instead of the changes in the mean climate state under the GHGs forcings. This is important "when one wishes to discuss changes in the occurrence of extreme events," such like floods, droughts, storm activities, etc., in response to the global warming (Stouffer and Wetherald 2007). The paper is structured as follows. Section 2 introduces the data, the coupled models, and experiments. Section 3 revisits the observations. Section 4 shows the ENSO properties and mean states in our coupled models. Section 5 investigates the mechanisms of the ENSO amplitude change through term balance analyses. Section 6 provides some conclusions and discussions on our results. The most important conclusion in this work is that we think the impact of global warming on ENSO properties cannot be neglected, and the mean state change in the ocean may play a deterministic role in the long-term changes in ENSO behaviors.

2. Data, model, and experiments

Observational datasets used here include 1) the Met Office Hadley Centre's monthly sea ice and SST dataset (HadISST) spanning the period January 1870 to June 2006 (Rayner et al. 2003) and 2) the monthly upper-ocean temperature dataset from the Joint Environmental Data Analysis Center (JEDAC-XBT) at the Scripps Institute of Oceanography, spanning the period 1955–2003. The HadISST has a horizontal resolution of $1^\circ \times 1^\circ$ covering the global oceans. The JEDAC data has a horizontal resolution of $5^\circ \times 2^\circ$ in longitude–latitude and 11 vertical levels from surface to 400 m (additional information is available online at http://jedac.ucsd.edu/DATA_IMAGES/index.html).

The model used in this study is the Fast Ocean Atmosphere Model (FOAM) developed jointly at University of Wisconsin—Madison and the Argonne National Laboratory (Jacob 1997). The atmospheric resolution is R15 with 18 vertical levels. The ocean resolution is 1.4° latitude $\times$ 2.8° longitude $\times$ 32 vertical levels. FOAM has been used extensively to simulate the global climate in the past, present, and future. Comprehensive analyses of the model simulation can be found, for example, in Wu et al. (2003) and Yang and Liu (2005).

The model experiments examined in this study are "1% increase per year to doubling" (1pctto2x) experiments. The "1pctto2x" runs are performed starting from a present-day control run with the 1990 CO_2 level of 355 ppmv. The model is integrated with a 1% yr^{-1} increase in CO_2 for 70 yr when the CO_2 concentration is doubled. Then the model is integrated for additional 150 yr with the fixed double CO_2. In this paper, the transient 1% CO_2 simulation is referred as 2CO2T, while the equilibrium double CO_2 simulation is referred as 2CO2E. To reduce model uncertainty, six-member ensemble "1pctto2x" simulations are performed, starting from different time in their present-day control runs. For the convenience of comparison, six-member ensemble control runs are continued for another 120 yr. In the following context, only the ensemble mean results are analyzed.

The responses of the ocean–atmosphere system to different stages of climate warming are expected to be different. This work will compare the ocean and atmosphere status in different stages and try to reveal the mechanisms responsible for these differences. The monthly anomalous variables are obtained as follows. First, the mean seasonal cycle of each variable is removed. Second, the secular linear trend is subtracted. Third, a bandpass filter of 5–85 months is further applied so that the resultant variabilities only contain ENSO time-scale information. Both the high-frequency variability and the decadal fluctuation of the background state have been excluded. These quantities are also brought in the temperature variance equation to calculate the terms (see appendix).

3. Observations

a. Change in ENSO amplitude

The ENSO amplitude has been changing in the past century as shown in Fig. 1a. The standard deviation

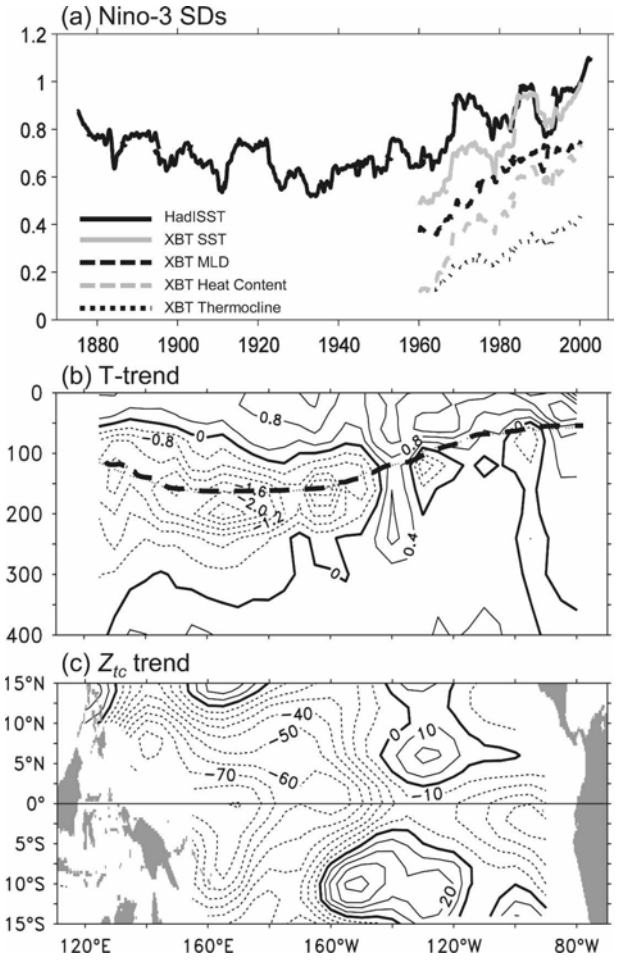

FIG. 1. (a) Time series of standard deviation (SD) of SST anomalies from HadISST and JEDAC-XBT and SD of mixed layer depth (MLD, m), upper-ocean heat content (10^9 W m^{-2}), and temperature anomalies (°C) averaged between 40 and 400 m from JEDAC-XBT over the Niño-3 region (5°S–5°N, 150°–90°W). The anomalies have been detrended and bandpass filtered (5–85 months). The SDs are calculated from anomalies by applying a low-pass filter with a sliding window of 11 yr. Linear trends of (b) the upper-ocean temperature (°C century^{-1}) averaged between 5°S and 5°N and (c) the equatorial thermocline depth Z_{tc} (m century^{-1}) from JEDAC-XBT over the period 1955–2003. The dashed thick line in (b) represents the mean thermocline depth Z_{tc}, which is defined as the location of the maximum vertical temperature gradient.

(SD) of Niño-3 SST anomaly is around 0.7°C before 1900. It reaches the minimum (0.6°C) during the 1940s and then increases to around 0.9°C during the past two decades, showing a nearly 50% increase in the ENSO variability. This increase in ENSO amplitude is significant and passes the Student's t test of 95% significant level, although it does not appear as a smooth increase and exhibits some decadal variability. It is noticed that there is a suspicious SD "spike" near year 2000 (Fig. 1a). This is influenced by the strong El Niño event in 1997/98, because the SD is calculated with an 11-yr sliding window. We also calculated the SD with 21- and 31-yr sliding window (figure not shown). The rising in ENSO amplitude after 1940s is remarkable and is insensitive to the width of the sliding window. The increasing interannual variabilities can be also seen in the mixed layer depth, the thermocline temperature, and the upper-ocean heat content in JEDAC-XBT data (Fig. 1a).

b. Changes in mean climate

Consistent with the enhancing ENSO amplitude since 1940s, the Pacific equatorial thermocline also shows a strengthening trend (Fig. 1b). The warming rate of tropical SST in the past 50 yr is generally over 1°C century^{-1}; it reaches 1.5°C century^{-1} in the eastern equatorial Pacific. This big surface warming, however, does not appear to penetrate downward into the thermocline, where a cooling trend occurs instead. The cooling rate in the western equatorial Pacific reaches as much as -2°C century^{-1}. Although the cooling rate in the eastern thermocline is not as significant as that in the west, the overall vertical temperature gradient is enhanced substantially during the past 50 yr. In contrast to the thermocline strength, the observation shows a clear reduction in the mean depth of equatorial thermocline (Z_{tc}) during the same period (Fig. 1c). The shoaling trend of Z_{tc} is not uniform along the equator. It is more notable in the western equatorial Pacific than in the east. This pattern also suggests a flattening in the east–west tilt of the equatorial Pacific thermocline.

The strengthened thermocline appears to be responsible for the shift in ENSO amplitude as suggested by many coupled model studies (e.g., Meehl et al. 2001; Collins 2000; Timmermann et al. 1999). The shoaling of Z_{tc} is likely to increase the SST sensitivity to the thermocline, especially in the Niño-3 region (Philip and van Oldenborgh 2006). A shallower Z_{tc} in the equatorial Pacific suggests that the local mode or SST mode, resulting from local SST–wind interaction in the central-east Pacific, may play a relatively important role in generating ENSO variability (Fedorov and Philander 2001; Guilyardi 2006). This local mode is described as the anomalous upwelling of the mean temperature gradient ($-w'\overline{T}_z$) in the SST equation. A shallower Z_{tc} means the thermocline water would be easier to affect the SST through the anomalous upwelling (w'). A stronger thermocline ($\overline{T}_z$) means a bigger impact on SST. Here, the w' is closely related to the local wind variability and bridges the mean thermocline with the SST variability. The observation shows that the mean SST increases the

most in the Niño-3 region (Fig. 1b), where an increasing response of winds to SST variability is expected (Philip and van Oldenborgh 2006). Therefore, the shallower and stronger thermocline could result in an enhanced ENSO variability because of the positive feedback among the wind variability, anomalous upwelling, and SST variability in the central-east Pacific. This speculative discussion will be examined thoroughly in the next section through term balance analyses on coupled model experiments.

The shoaling and flattening of the equatorial thermocline can be attributed to the weakened trade wind, and thus the weakening of tropical Walker circulation (Vecchi et al. 2006; Vecchi and Soden 2007). Coupled models' studies have suggested that these changes in atmosphere in the past century may result from anthropogenic forcing (Vecchi et al. 2006). A consequence of the weakened trade wind is to stabilize the tropical atmosphere–ocean coupling system (Vecchi et al. 2006; Meehl et al. 2001; Neelin et al. 1992; Clarke and Lebedev 1996), which would result in the suppression of the ENSO variability. Many sensitivity studies of linear and coupled models (Fedorov and Philander 2001; Meehl et al. 2001) have shown the similar conclusions.

However, the enhanced ENSO variability suggests that the stabilizing effect of atmosphere does not seem to compensate the destabilizing effect of the enhanced thermocline completely in the past half century. We therefore speculate that the ocean, particularly the subsurface ocean, may play a more important role in the long-term changes of ENSO properties. Some studies have shown a poor relationship between the shift in ENSO activity and the mean climate change during the last millennium (Cobb et al. 2003). Yet the mean climate change in the past century is so obvious that its impact on the ENSO behaviors should be paid attention sufficiently. The mean climate change in the ocean may even overwhelm the influence of atmosphere change, as implied in the observations.

The ENSO behavior during the transient warming period, like the twentieth century, does not imply that it will behave the same in a warmed climate. Although the mean atmosphere climate during the transient period and equilibrium period could be very similar because of quick response of atmosphere to external forcings, the mean ocean climate could be very different because of the huge thermal inertia of the ocean. This could result in a different ENSO in a warmed climate. Our questions are: would the ENSO be changing in the whole global warming period? If so, how would the ENSO change? What does the role of the ocean play in the ENSO change? Next we will check the ENSO behavior in our coupled model experiments.

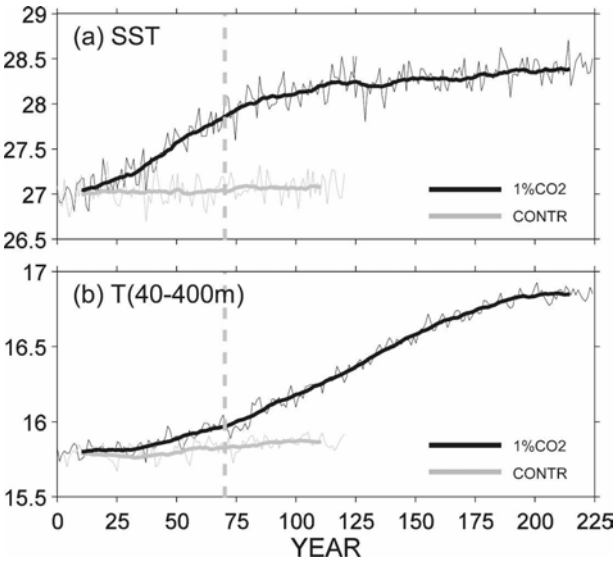

FIG. 2. Time series of (a) SST and (b) upper-ocean temperature (40–400-m averaged) in the tropical Pacific in control run (gray line) and 1% CO_2 run (black line). The thick lines are the 21-yr running mean of the thin lines. The temperature is averaged between 10°S and 10°N of the whole tropical Pacific (120°E–80°W). Doubling of CO_2 occurs at year 70 and is denoted by the thick dashed gray line.

4. Coupled model results

Changes in mean climate and ENSO amplitude

The equatorial SST increases almost linearly under the forcing of the transient increasing of CO_2 (Fig. 2a) as expected in most coupled models. At year 70 when the CO_2 concentration is doubled, the equatorial SST has been warmed by about 1°C. Afterward, under the forcing of fixed double CO_2, the SST changes very slowly and is only warmed by about 0.4°C from year 71 to year 220. In contrast to the SST, the equatorial thermocline is only warmed by about 0.3°C during the transient forcing period (Fig. 2b). This warming rate is obviously much smaller than that in SST. However, during the equilibrium forcing period, the warming rate in the thermocline is, in turn, much larger than that in SST. The thermocline temperature has been warmed by about 0.8°C from year 71 to 220. This situation suggests that the ocean climate change will persist for a much longer time than the atmosphere, even after the external forcings stop changing. It further implies that the ocean–atmosphere coupled variabilities, which are closely related to the mean states of both the atmosphere and ocean, may behave differently during the different stages of climate change.

The coupled tropical variabilities, for example, the ENSO variability, do show big variations during the whole global warming period (Fig. 3). Compared with

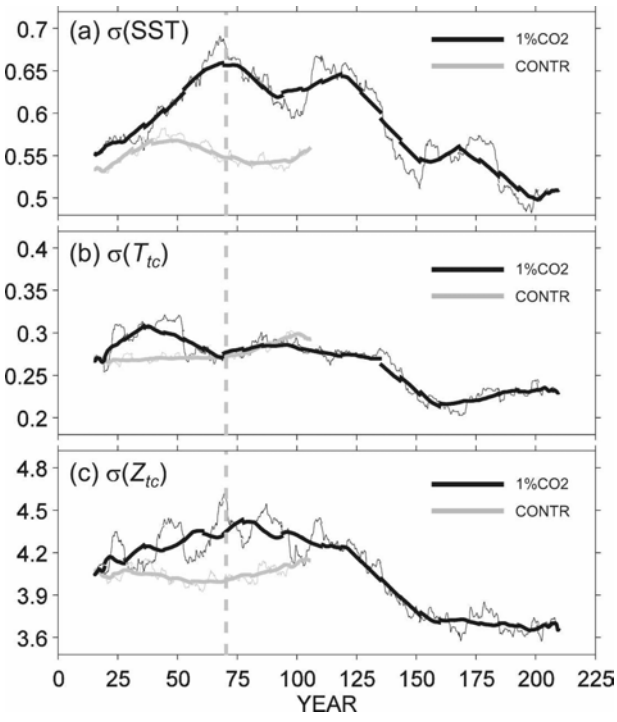

FIG. 3. Time evolutions of SDs for the Niño-3 region (a) SST (°C), (b) temperature at the thermocline depth, and (c) thermocline depth (Z_{tc}, m) anomalies for control run (gray lines) and 1% CO_2 run (black lines). A low-pass filter with a sliding window of 31 yr is used to calculate the SD. The thick lines are 31-yr running mean version of the thin lines.

the control run, the time evolution of the tropical temperature SD shows a much bigger oscillation (An et al. 2008). During the transient period, the Niño-3 SST SD appears to increase with time (Fig. 3a). The mean SST SD averaged over years 50–70 is around 0.64°C, showing a near 16% increase in amplitude when compared to the mean variability in control run (0.55°C). During the equilibrium period, the Niño-3 SST variability is, in turn, reduced significantly. The mean SD averaged over the last 50 yr (years 170–220) is about 0.53°C, showing a 4% reduction when compared to the control run, or a 17% reduction when compared to that in the transient period (0.64°C). The same situation also occurs in the equatorial thermocline, such as the temperature variability at the mean thermocline depth Z_{tc} (Fig. 3b), as well as the thermocline variability (Fig. 3c) defined as the SD of the thermocline depth anomaly (Z_{tc}'). They both show a modest increase in the transient stage and a clear decrease in the equilibrium stage when compared to those in the control run.

The turnaround in the interannual variability, enhancing during the transient stage and then weakening during the stable stage, occurs almost in the entire tropical Pacific. In normal conditions, the ENSO variability shows bigger amplitude in the eastern equatorial Pacific for both the SST and thermocline in our control run (Figs. 4a,b). During the transient stage of global warming, the SST variability is enhanced significantly in the tropics, despite the nonuniformity in the spatial pattern (Fig. 4c). The thermocline depth variability shows a modest increase in the eastern and southern Pacific and a weak decrease in the western equatorial Pacific (Fig. 4d). During the equilibrium stage the remarkable decrease in ENSO variability occurs in the thermocline (Fig. 4f), showing a 20% reduction relative to control run. The SST variability also shows a 5%–10% decrease in the eastern Pacific (Fig. 4e).

The spatial pattern of ENSO mode simulated in our model appears to be unaffected, despite the notable changes in ENSO time-scale variability. The ENSO mode is defined as the first EOF mode of the tropical SST anomaly within 25° of the equator, which accounts for about 18% of the total SST variance (Fig. 5a) and has a principal period of around 30 months in the control run (Fig. 5b). The ENSO mode has the maximum amplitude located in the central equatorial Pacific (Fig. 5a), which is partly due to the overwestward spread of the equatorial cold tongue in our coupled model. This pattern does not change in 2CO2T and 2CO2E (figure not shown). The first EOF mode in Fig. 5a can be thought as the "real" ENSO mode, while the SD of tropical SST in Fig. 4a can be thought of as ENSO time-scale variability. These two are not exactly the same. The latter is clearly changed in the CO_2 experiments as shown in Figs. 4c,e, which may result from the changes in the higher-order modes of the tropical SST. These higher-order modes still have time scales within 5–85 months.

The power spectrum of the time series of the first ENSO mode (Fig. 5b) is also checked. The principal period of 30 months in control run does not change in 2CO2T, but it seems to shift toward both the longer and shorter period in 2CO2E. Moreover, in 2CO2T, besides the 30-month period, there is another significant peak at about 20 months. In addition, the global warming seems to favor more high-frequency variabilities with periods shorter than 20 months. Figure 5b also shows that the power of ENSO mode in 2CO2E is less than that in 2CO2T and control, consistent with the discussions in Figs. 3 and 4. The frequency change itself in response to global warming is a very complex problem. It is unlikely to elucidate this problem in our current work. We will study this question with more ensemble experiments and more coupled models in the near future.

In general, our coupled model experiments show a big variation in ENSO amplitude during the entire

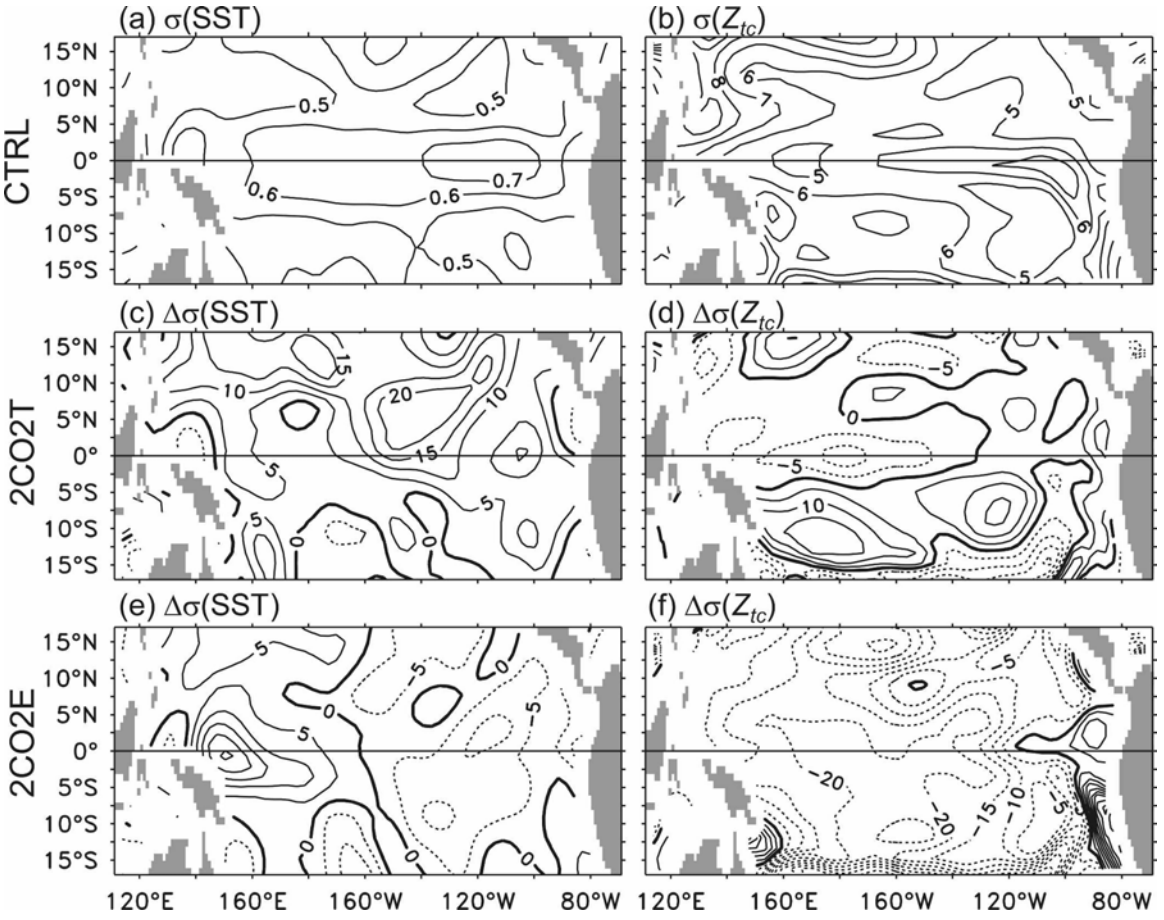

FIG. 4. Spatial patterns of the SDs of the tropical (a) SST (°C) and (b) thermocline depth (Z_{tc}, m) anomalies in control run. (c), (d) Percentage changes of the SD in (left) SST and (right) Z_{tc} in 2CO2T. (e), (f) Same as (c), (d) but for 2CO2E. The anomalies are 5–85-month bandpass filtered before calculating the SD. The percentage change is calculated as the SD difference between warming experiments and control run divided by that in control (unit in %).

global warming period. Previous studies have established a robust connection between the ENSO properties and the tropical mean ocean–atmosphere climate, particularly between the ENSO amplitude and the equatorial thermocline strength as shown in the observations (Fig. 1). The model experiments show a strengthened vertical stratification along the equator in 2CO2T (Fig. 6c) consistent with the enhanced ENSO amplitude. It is seen that, in this stage, the warming effect of the atmosphere forcing has very limited downward penetration. Most of the warming is confined in the upper thermocline above 200-m depth. The temperature in the lower thermocline is only slightly increased. There is even a small cooling at 200–300 m in the western Pacific. After another 150-yr evolution, the lower thermocline finally warms up and the temperature rises by 0.9°C (Fig. 6d). During the equilibrium stage, the sea surface is only warmed by 0.2°C (Figs. 6a,b), while the lower thermocline is warmed by 0.7°C. Therefore, the equatorial vertical stratification is, in turn, weakened considerably, which is consistent with the weakened ENSO amplitude in this stage.

The cooling or minimum warming in the western thermocline (Figs. 6c,d), which is also clear in the observation (Fig. 1b), may result from both the equatorial and off-equatorial processes. The weakened trade winds cause the flattening of the east–west thermocline slope, resulting in an upward movement of the deeper colder water. This may involve equatorial wave processes that span the width of the basin. In the global warming situation, there could also generate cold Rossby waves in the off equator, propagating westward and southward along the mean potential vorticity contours and cooling the western equatorial thermocline (Yang et al. 2005). Other coupled models forced by increasing GHGs have also shown the cooling thermocline in the equator (Timmermann et al. 1999; Zhang et al. 2008).

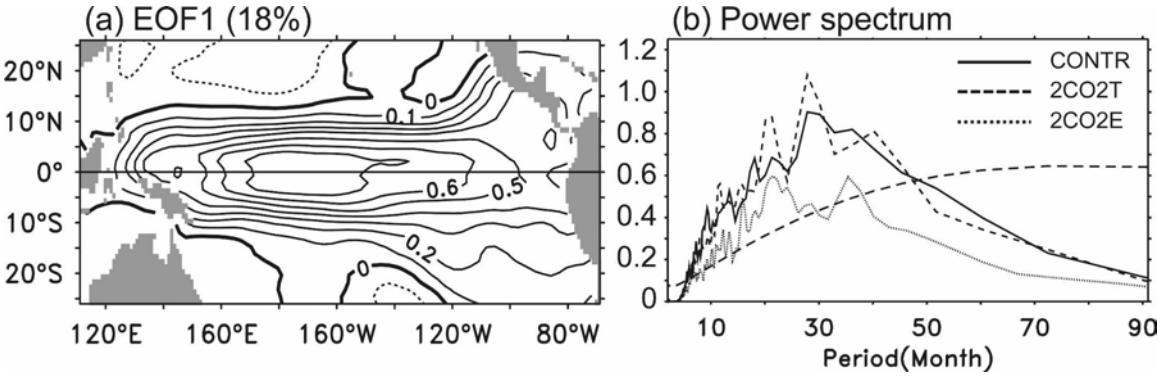

FIG. 5. (a) The first EOF mode of the tropical SST anomaly within 25° of the equator in control run and (b) the power spectrums of the time series of the first EOF mode for control (solid), 2CO2T (dashed), and 2CO2E (dotted). The vertical coordinate in (b) is transformed as the ratio of power over period and further normalized. The 90% confidence level is plotted as the long dashed line in (b).

The tropical atmosphere in our experiments experiences reductions in the east–west sea level pressure (SLP) gradient and equatorial trade winds (Fig. 7). This suggests a slowdown of Walker circulation during the entire global warming period, similar to that in observation and other models (Vecchi et al. 2006; Vecchi and Soden 2007). The pattern in Fig. 7b is very similar to that in Fig. 7c, except small differences in the magnitude of SLP and wind anomalies. This is understandable because the atmosphere and the SST change swiftly in response to the CO_2 forcing so that they can reach dynamical equilibrium in a short time. These mean climate change in atmosphere are thought as to suppress the ENSO variability in many studies. There-

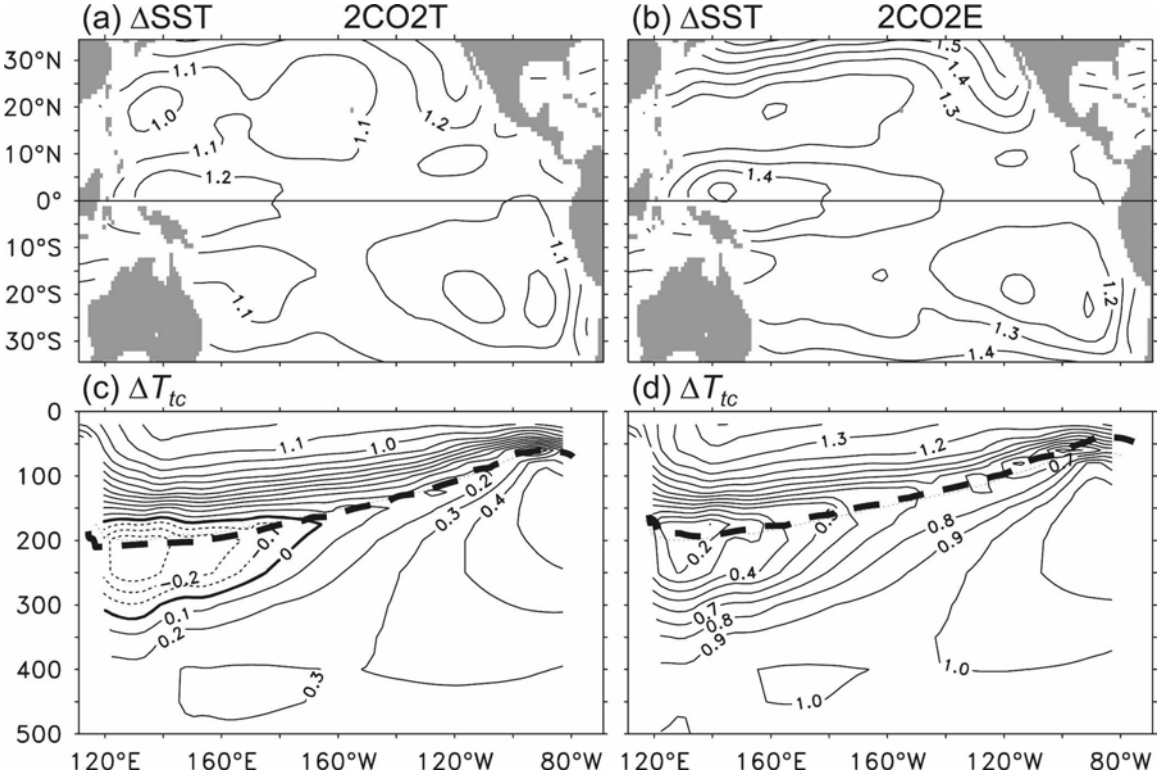

FIG. 6. Mean temperature changes in (a), (b) SST and (c), (d) the upper-equatorial Pacific averaged between 5°N and 5°S for (left) 2CO2T and (right) 2CO2E. The thick dashed lines in (c) and (d) represent the location of mean Z_{tc}. The temperature anomalies in (a) and (c) are obtained by subtracting the mean temperature over year 50–70 in 2CO2T from the control run.

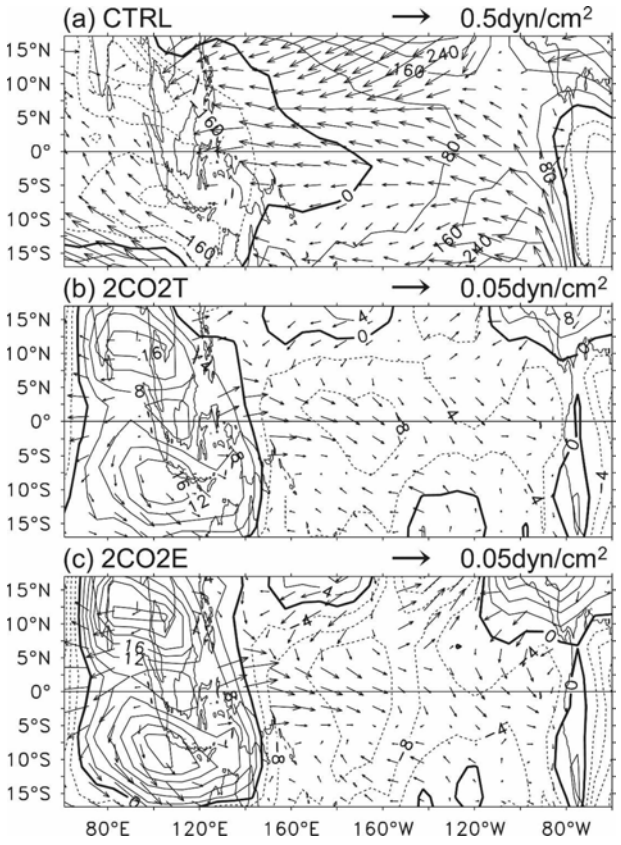

FIG. 7. (a) Mean SLP (Pa) and sea surface winds (dyn cm^{-2}) in the tropical Indo-Pacific Ocean in the control run and their changes in (b) 2CO2T and (c) 2CO2E. The zonal mean SLP is removed in (a)–(c).

fore, the turnaround of the ENSO amplitude can be due to the delayed response of the ocean to global warming (An et al. 2008). This increases the complexity and uncertainty when assessing the ENSO behaviors in global climate change.

The above descriptions on the ENSO amplitude change in different global warming stages are highly qualitative. Next we will investigate the mechanisms and the dynamic processes through term balance analyses on the equation of temperature variance.

5. Mechanisms

a. Term balance analyses for control run

To identify the dynamic processes that are responsible for the temperature change, the terms in the temperature equation are carefully examined (see the appendix). The temperature tendency is controlled by advection terms, external forcing terms, and damping terms. For the equilibrium state, the mean temperature change is nearly zero, so the terms above are well balanced. For the equatorial Pacific surface, the downward heating of the surface net heat flux ($\overline{Q}_F > 0$) is mainly balanced by the cooling effects of poleward heat transport of the Ekman flow ($-\overline{v}\overline{T}_y < 0$) and the Ekman upwelling ($-\overline{w}\overline{T}_z < 0$). For the subsurface ocean, the temperature is maintained by the equatorward heat transport of the geostrophic flow ($-\overline{v}\overline{T}_y > 0$), the Ekman upwelling ($-\overline{w}\overline{T}_z < 0$), and the vertical temperature diffusion ($A_v\overline{T}_{zz} < 0$). These have been discussed in Yang and Liu (2005).

From the temperature anomaly equation (A3), the relative importance of the terms on the right side of (A3) can be identified in principle. However, since all the anomalous terms in (A3) oscillate around their own mean values over the time, the time means of these terms tend to be zero. Thus in practice it is inconvenient to assess the time-averaged contributions of the terms to the amplitude of temperature anomaly. Here we derive the equation for temperature variance (A7), in which the anomalous terms are nonlinear so that their time means are nonzero. Based on (A7), the contributions of each term to the temperature amplitude can be explicitly estimated. The dominant mechanisms of the temperature amplitude change can thus be easily pinpointed.

Different from the processes controlling the mean temperature, the temperature amplitude change is mainly determined by the balance between the vertical temperature advection, the vertical temperature diffusion, as well as the meridional advection and diffusion terms. Here we first discuss the results from the control run. The most important driving mechanism for the amplitude of Niño-3 temperature anomaly is the vertical advection term $[-T'(w'\overline{T}_z + \overline{w}T'_z)]$ (Fig. 8a). The largest damping effect comes from the vertical temperature diffusion $[A_vT'T'_{zz}]$. The secondary damping processes are the meridional advection term $[-T'(v'\overline{T}_y + \overline{v}T'_y)]$ and diffusion term $[A_hT'T'_{yy}]$. The zonal advection and diffusion terms are very small and negligible. For a steady state without amplitude change, these terms have to be balanced. Here we would like to emphasize that the terms in Fig. 8 are calculated at the time mean thermocline depth Z_{tc}. Before the calculation, all variables, including the derived quantity like vertical temperature gradient T_z, have been interpolated to the depth Z_{tc}. The term balance at Z_{tc} can also represent the situation above the thermocline, except the thin sea surface level. The vertical advection term is underestimated on the sea surface (figure not shown), because both the vertical movement w and the vertical temperature gradient T_z are very small at the sea surface. The small w is resulted from the rigid-lid approximation in the ocean model. The T_z is small because, technically, it is calculated within the mixed layer. But

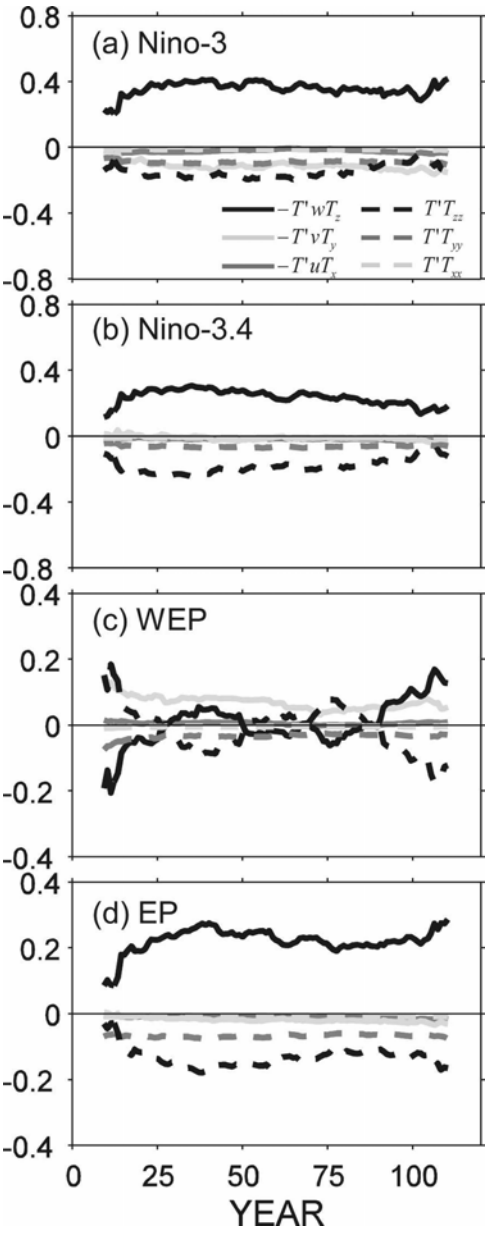

FIG. 8. Time evolution of the terms in the temperature variance equation for the control run, averaged for the equatorial Pacific Ocean at the thermocline depth: for (a) the Niño-3 region, (b) the Niño-3.4 region (5°S–5°N, 190°–240°E), (c) the western equatorial Pacific (5°S–5°N, 120°–160°E) and (d) the whole equatorial Pacific (10°S–10°N, 140°–280°E). The solid black, light gray, and heavy gray lines are for the vertical, meridional, and zonal temperature advection ($-T'wT_z$, $-T'vT_y$, and $-T'uT_x$), respectively. The dashed light gray and heavy gray lines are for the horizontal mixing terms ($A_hT'T'_{xx}$, $A_hT'T'_{yy}$), and the dashed black line is for the residual term, which mainly represents the vertical temperature diffusion ($A_vT'T'_{zz}$) in the equatorial Pacific. These lines are smoothed with a 21-yr sliding window. Before the calculation of these terms, all variables (like T, u, v, and w) are filtered with a 5–85-month bandpass filter. The unit of these terms is 10^{-8}°C^2 s^{-1}.

physically both the T_z and upwelling w are important to the SST, at least in the eastern equatorial Pacific.

The above analyses are valid for the most of the equatorial Pacific. An exception occurs in the warm pool region, in which the vertical term is very small while the meridional advection term dominates the amplitude change of temperature anomaly (Fig. 8c), because both the upwelling and temperature stratification here is much weaker than in the east. However, the vertical advection term is the most important destabilizing factor to the changes in the amplitude of the temperature variability for the equatorial Pacific Ocean on the whole (Figs. 8a,b,d).

Here let's focus on the dynamic effect of the vertical advection term on the amplitude of interannual variability in the equatorial Pacific. This term can be further decomposed into three subterms: 1) the local term which depicts the anomalous upwelling of the mean temperature $[-T'w'\overline{T}_z]$ (see the appendix; Fedorov and Philander 2001; Guilyardi 2006), 2) the remote term which represents the mean upwelling of the anomalous temperature gradient $[-T'\overline{w}T'_z]$ (Fedorov and Philander 2001), and 3) the nonlinear term $[-T'w'T'_z]$. These subterms are closely related to the vertical temperature gradient.

For the FOAM control run, in the Niño-3 region the local term dominates over the remote term and plays a more important role in the amplitude of the temperature variability. Figure 9a clearly shows that the time evolution of the local term (gray line) follows tightly with that of the total vertical advection term (black). It acts as a positive factor that favors an increase in temperature variability around the thermocline. The remote term (dashed black) varies in the vicinity of zero and its time mean value is slightly less than zero, which acts as a weak damping effect. The nonlinear term (dashed gray), as expected, is negligible.

The local term is proportional to the mean vertical temperature gradient ($\overline{T}_z$), where the latter plays as a "background" of the perturbation quantities such like the anomalous upwelling (w') and temperature anomaly (T'). Figure 9d shows that, although the w' and T' themselves oscillate around zero over the time, the product of w' and T' ($-w'T'$, thick black), after a low-pass filtering, is well elevated from the zero. Therefore, besides the background temperature gradient ($\overline{T}_z$), the $-w'T'$ is also crucial to the sign and the final magnitude of the local term. Here the positive $-w'T'$ in Niño-3 region can be understood as follows. Under the background of positive temperature gradient ($\overline{T}_z > 0$), an anomalous upwelling ($w' > 0$) can bring cold water at depth upward, and cause a negative temperature anomaly tendency ($T'_t < 0$) based on Eq. (A3). For

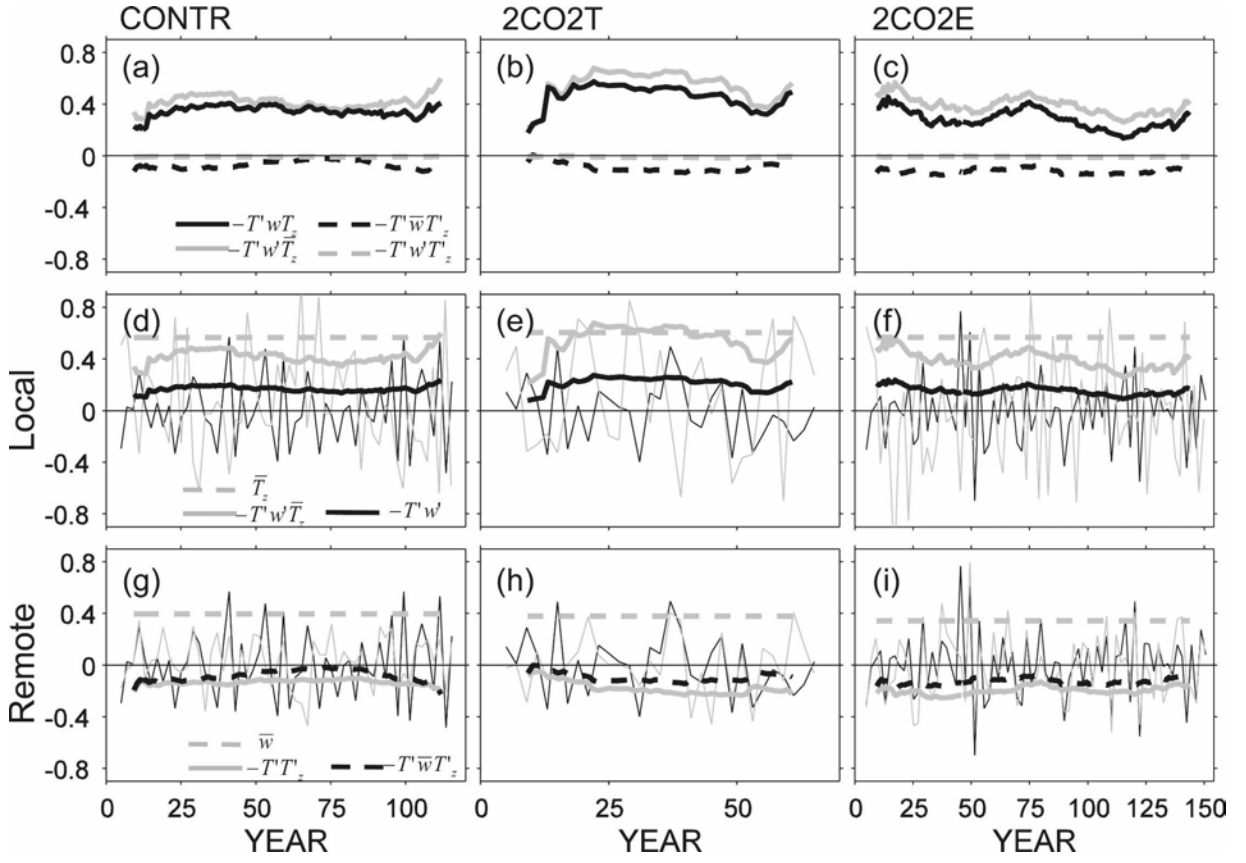

FIG. 9. Decomposition of the vertical temperature advection term averaged over the thermocline of Niño-3 region for (left) control run, (center) 2CO2T, and (right) 2CO2E. (a)–(c) The solid black, solid gray, dashed black, and dashed gray lines represent the total vertical temperature advection ($-T'wT_z$), the perturbation upwelling of mean temperature gradient ($-T'w'\overline{T}_z$), the mean upwelling of perturbation temperature gradient ($-T'\overline{w}T'_z$), and the pure nonlinear term ($-T'w'T'_z$), respectively. (d)–(f) The thick solid black, solid gray, and dashed gray lines represent vertical heat flux ($-w'T'$), $-T'w'\overline{T}_z$, and mean vertical temperature gradient ($\overline{T}_z$). The thin solid black and gray lines represent the anomalous temperature (T') and upwelling (w'), respectively. (g)–(i) The thick solid gray, dashed gray, and dashed black lines represent $-T'T'_z$, mean upwelling ($\overline{w}$), and $-T'\overline{w}T'_z$, respectively. The thin solid black and gray lines represent T' and anomalous temperature gradient (T'_z). Same as in Fig. 8, all those thick lines are smoothed with a 21-yr running mean. In (a)–(c), the unit of terms is 10^{-8}°C^2 s^{-1}. In (d)–(i), the terms are scaled by a factor of certain constant so that they can be plotted in the same figure. The units of T', w', and T_z are °C, m s^{-1}, and °C m^{-1}, respectively. The real values of T', w', $\overline{w}$, T'_z, $\overline{T}_z$, $w'T'$, and $T'T'_z$ are the plotted values multiplied by 0.5, 3×10^{-7}, 10^{-5}, 5×10^{-3}, 0.2, 10^{-7}, and 10^{-3}, respectively.

an initially cold water ($T' < 0$), an anomalous upwelling ($w' > 0$) can enhance the initial anomaly so that the $-w'T' > 0$. An anomalous downwelling ($w' < 0$) can damp the initial cold anomaly quickly and finally produce a warm anomaly ($T' > 0$). The further check on the relationship between w' and T' confirms that they are negatively correlated (Fig. 10, black). The peak correlation occurs when T' lags w' by 3 months, with the maximum correlation of about -0.5. This suggests that the upwelling (downwelling) can cause cold (warm) anomaly. Although there is a time lag between w' and T', the low-pass filtered $-w'T'$ is generally above the zero. The $-w'T'$ can be somehow thought as the vertical heat flux and should also correlate positively with the mean temperature gradient. The local upwelling w' is closely related to the wind-driven Ekman pumping w'_e, that is, the zonal wind stress anomaly τ'_x. Figure 10 shows that there is no time lag between w' and w'_e (dashed black line). The maximum positive correlation is about 0.4.

The remote term is determined by the product of the mean upwelling ($\overline{w}$), temperature anomaly (T') and the anomalous vertical temperature gradient (T'_z). Although the $\overline{w}$ is much larger than the w' in the local term, the T'_z is much smaller than the $\overline{T}_z$ in the local term. The ratios of $w'/\overline{w}$ and $\overline{T}_z/T'_z$ are usually around 10^{-2} and 10^2, respectively. The remote term and the local term could be comparable if the $\overline{T}_z$ is not that strong. In our experiments, the mean depth of the equatorial thermocline is relatively shallow, particularly in

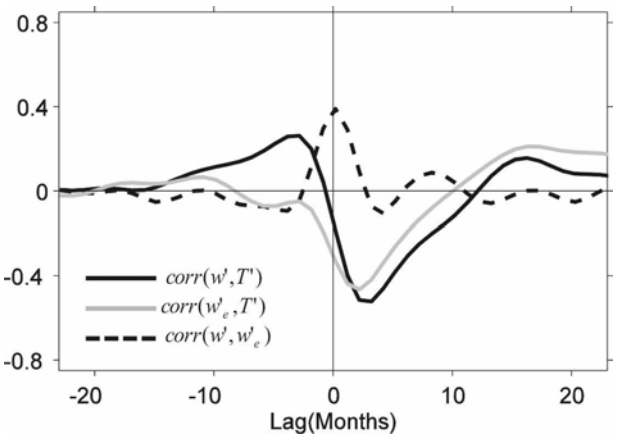

FIG. 10. Lag correlations among anomalous temperature (T'), upwelling (w'), and Ekman pumping (w'_e) over the thermocline of the Niño-3 region for control run. The black, gray, and dashed black lines represent the correlation between w' and T', w'_e and T', and w' and w'_e, respectively. The Ekman pumping w'_e is calculated from the surface wind stress. The positive month means the time that T' lags w', T' lags w'_e, and w'_e lags w', respectively. All variables are filtered with a 5–85-month bandpass filter before calculating correlation.

the eastern Pacific (dashed thick line in Fig. 6c). This is usually associated with a strong $\overline{T}_z$, and favors an easy and quick interaction between the local surface air and the thermocline water. The equatorial unstable modes can be thus thought as the local modes or the SST mode that have been discussed in Fedorov and Philander (2001; i.e., the modes in the vicinity of point E in their Fig. 4). The local term, or the local air–sea coupling plays a dominant role in the temperature variation. This can also explain why the T' and w' in Niño-3 region tends to be out of phase despite the time lag between them (Figs. 9d and 10). A deep thermocline, however, means that the $\overline{T}_z$ near the surface would be very weak so that the remote term $\overline{w}T'_z$ has to be dominant (Fedorov and Philander 2001).

b. Changes in term balance under global warming

The enhanced ENSO variability during the transient period of global warming results from the bigger local term. Figures 9b and 11a explicitly show the elevated vertical advection term and its local component. Compared with the mean value (0.43) in the control run, the local term is increased by 21% to 0.52 in 2CO2T (gray line in Fig. 9b). The contributions to the increased local term come from the mean vertical temperature gradient $\overline{T}_z$, which is enhanced by 7% to 0.61 in 2CO2T (Figs. 9e and 11a) from 0.57 in control run (Fig. 9d), as well as the "virtual vertical heat flux" $-w'T'$, which is increased by 17% to 0.21 in 2CO2T from 0.18 in control run. (For simplicity the values discussed here are the plotted values in Fig. 9. The real values should be multiplied by certain constants. See the Fig. 9 caption for the details.) It is noticed that the contribution of $-w'T'$ to the increased local term is clearly larger than that of $\overline{T}_z$. This does not have to impair the critical role of $\overline{T}_z$ in ENSO amplitude change. Because the $\overline{T}_z$ can be

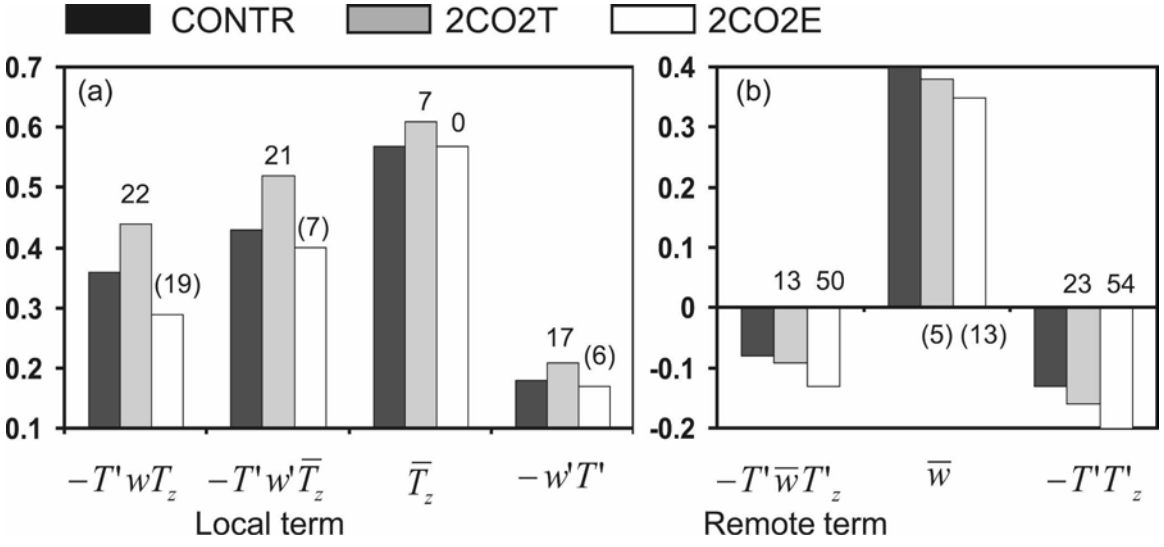

FIG. 11. Bar diagram showing the mean values of the vertical temperature advection term and its components averaged over the thermocline of the Niño-3 region. (a) The total advection $-T'wT_z$, $-T'w'\overline{T}_z$, $\overline{T}_z$, and $-w'T'$; (b) $-T'\overline{w}T'_z$, $\overline{w}$, and $-T'T'_z$. The dark bars are for the control, the gray bars for the 2CO2T, and the blank bars for the 2CO2E. The average is over years 1–120 for the control, years 50–70 for the 2CO2T, and years 170–220 for the 2CO2E. The numbers above the bars represent the percentage changes in the 2CO2T and 2CO2E to the control run, in which the numbers in parenthesis mark show negative changes. The real values of $-T'wT_z$, $\overline{T}_z$, $-w'T'$, $\overline{w}$, and $-T'T'_z$ are the plotted values multiplied by 10^{-8}, 0.2, 2×10^{-7}, 10^{-5}, and 2×10^{-3}, respectively.

viewed as the background state of $-w'T'$, and, the magnitude of $-w'T'$ should be positively correlated to the strength of $\overline{T}_z$.

The reduced ENSO amplitude during the equilibrium stage is associated with the reduced local term (Fig. 9c). The mean values of the local term, $\overline{T}_z$ and $-w'T'$ over the last 50 yr of 2CO2E are 0.40, 0.57, and 0.17 (Fig. 9f), which are reduced by 23%, 7%, and 19%, respectively, when compared with those in 2CO2T. It is noticed that these terms change little when compared with the control run (Fig. 11a). It is unnecessary that they should be smaller than those in the control run. In this study we focus on the different behaviors of ENSO in different stages of global warming. The ocean in the 2CO2E does act differently from that in the 2CO2T.

The remote term exerts a weak damping effect on the ENSO amplitude. It is much smaller than the local term (Figs. 9a–c). Consistent with the changes in mean trade wind (Fig. 7), the mean upwelling $\overline{w}$ in the remote term is reduced to 0.38 in the 2CO2T, and further to 0.35 in the 2CO2E (Figs. 9g–i and 11b) from 0.40 in the control run. The weak mean upwelling implies a weak interaction between the thermocline and the surface. The $-T'T'_z$ in the remote term, which can be rewritten as $-(T'^2/2)_z$, represents the vertical gradient of the temperature variability. Usually the $(T'^2)_z > 0$ because the temperature variability in the shallower layer is larger than that in the deeper layer (Figs. 3a,b), so $-(T'^2/2)_z < 0$ as shown in Figs. 9g–i. Here it is plausible that the $(T'^2)_z$ determines the sign and size of the remote term. However, under the background of weak mean upwelling, the weak interaction between the thermocline and the surface would result in a large vertical gradient of the temperature variability $(T'^2)_z$. The $(T'^2)_z$ appears to be determined by and very sensitive to the $\overline{w}$. Therefore, although the weaker $\overline{w}$ tends to reduce the damping effect of the remote term and favors an increase in the temperature variability, the much stronger $(T'^2)_z$ can ultimately result in the stronger damping, where the background $\overline{w}$ determines the magnitude of $(T'^2)_z$. It is clearly seen that in Fig. 11b the $\overline{w}$ is reduced by 5% in the 2CO2T and 13% in the 2CO2E, while the magnitude of $-T'T'_z$ is increased by 23% in the 2CO2T and 54% in the 2CO2E, when compared with the control run. This increases the magnitude of remote term by 13% in the 2CO2T and 50% in the 2CO2E. Here the physical process of the remote term can be understood as that the mean upwelling brings the low variability water upward and thus causes a reduction in the magnitude of surface variability. In this sense the remote term tends to always play a damping role in the surface variabilities. Since the mean upwelling $\overline{w}$ is closely related to the large-scale atmosphere, for instance, the mean surface trade winds and the Walker circulation, the remote term, to some extent, manifests the effect of atmosphere change on the temperature variability in the tropics.

The relative changes of the vertical temperature advection and its subterms in global warming experiments are summarized in Fig. 11. In general, the enhanced ENSO variability in the 2CO2T results from the strengthened equatorial thermocline because of the sluggish subsurface ocean. This overwhelms the damping effect of the weakened equatorial trade winds or the mean upwelling. The turnaround in ENSO variability in the 2CO2E occurs because of the turnaround of the $\overline{T}_z$ and the bigger damping effect from the remote term as well. The ocean virtually plays a deterministic role in the ENSO amplitude in the whole global warming period.

The ocean role can be further understood from the sensitivity analyses on the tropical air–sea coupling (Fig. 12). The atmospheric sensitivity—the sensitivity of central equatorial zonal wind stress anomalies to the Niño-3 SST anomalies in the 2CO2T—changes little when compared with the control run (gray and dashed black lines in Fig. 12a). The atmospheric sensitivity in the 2CO2E over the last 50 yr even shows a decreasing trend (black line in Fig. 12a). Despite its decadal variation the mean value over the last 50 yr is very close to the control run. The oceanic sensitivity—the sensitivity of Niño-3 SST anomalies to the central equatorial zonal wind stress anomalies—increases in the 2CO2T (dashed black line in Fig. 12b). During the equilibrium period of global warming, the oceanic sensitivity is again reduced over the last 50 yr. These are well consistent with our conclusion that the ocean dynamics arising from the changing thermocline is responsible for the enhanced ENSO variability and its turnaround afterward. To further check the coupling between the surface SST and the thermocline, the sensitivity of Niño-3 SST to thermocline temperature anomalies and the contrary are calculated. The thermocline sensitivity to the Niño-3 SST changes little during the whole global warming period (dashed black and black lines in Fig. 12c). However, as expected, the sensitivity of Niño-3 SST to the thermocline temperature is enhanced in the 2CO2T and 2CO2E (Fig. 12d). These further highlight the deterministic role of the thermocline dynamics on the surface variability in the Niño-3 region. These sensitivities are calculated based on the zero lag correlation among SST, wind stress, and thermocline temperature. We have also calculated the sensitivities based on nonzero lag correlation (figure not shown). The largest sensitivities are found at the zero lag, and the sensitivities will reduce substantially and even become negative for nonzero lag correlations among them.

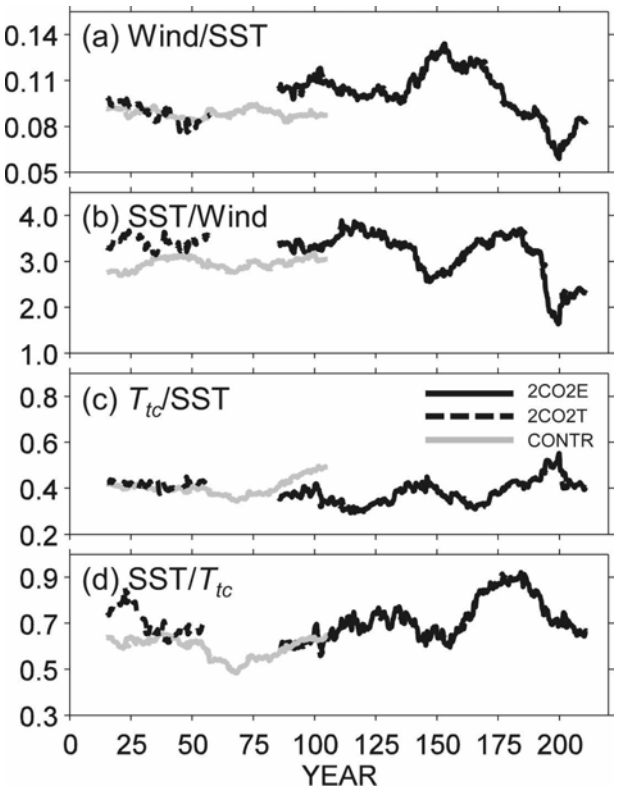

FIG. 12. (a) Sensitivity of central equatorial zonal wind stress anomalies (averaged over the region 5°S–5°N, 100°–160°W) to changes in the Niño-3 SST anomalies for (gray) control run, (dashed black) 2CO2T and (black) 2CO2E. The atmospheric sensitivity is defined as the covariance of the zonal wind stress and Niño-3 SST anomalies divided by the variance of the Niño-3 SST anomalies [(dyn cm^{-2}) °C^{-1}]. (b) The sensitivity of Niño-3 SST to the central equatorial zonal wind stress anomalies. The oceanic sensitivity is defined as the covariance of the zonal wind stress and Niño-3 SST anomalies divided by the variance of the zonal wind stress anomalies [°C (dyn cm^{-2})$^{-1}$]. (c) Sensitivity of Niño-3 thermocline temperature anomalies to changes in SST anomalies (°C °C^{-1}) and (d) sensitivity of Niño-3 SST anomalies to thermocline temperature anomalies (°C °C^{-1}). All variables are filtered with a 5–85-month bandpass filter before calculations. A sliding window of 31 yr is used to calculate the sensitivities.

The discussions above explicitly relate the vertical temperature gradient to the amplitude of the ENSO variability, in which we highlight the dominant role of the local term. However, the vertical temperature gradient in the equator does not have to be completely locally determined. It has to involve the meridional overturning circulation. As noted in the discussions in Liu and Yang (2003) and Yang and Liu (2005), the tropical–extratropical interaction affects the equatorial vertical thermocline structure to a great extent, particularly for the subsurface ocean where the mean advection mechanism plays an important role.

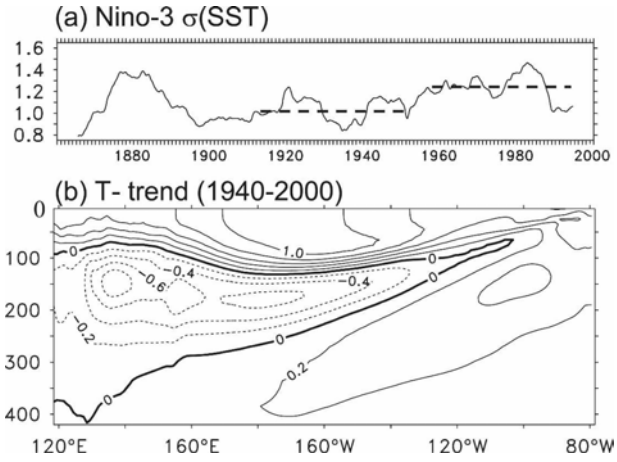

FIG. 13. (a) Time series of SD (°C) of Niño-3 SST and (b) linear trend (°C century^{-1}) of the upper-ocean temperature averaged between 5°S and 5°N over 1940–2000 for GFDL CM2.1 "20c3m" ensemble experiments. The dashed lines in (a) represent the mean SDs for period 1920–50 (1.05°C) and 1970–2000 (1.25°C), respectively. The anomalous data are similarly processed as in Fig. 1.

6. Summary and discussion

The discrepancy between the observed enhanced ENSO variability and the weakened equatorial trade winds in the past 50 yr brings our attention to the ocean. The equatorial thermocline dynamics appears to be more responsible for the ENSO variability. The strengthened equatorial stratification plays as a destabilizing factor that overwhelms the stabilizing effect of the slowdown of the Walker circulation and ultimately results in a stronger ENSO. Many previous studies have established a robust connection between the ENSO amplitude and the equatorial thermocline strength. This connection is, however, more or less qualitative. The explicit and quantitative connection between the ocean state and the ENSO variability or the air–sea coupling state, especially under the circumstance of the global warming, is yet to be specified.

To quantitatively explore the relationship between the ocean thermocline and the air–sea coupled variability, coupled model experiments are performed and the method of term balance analyses is used in this work. First of all we found that the statistical properties of the ENSO would change in the whole global warming period. It will change from a stronger ENSO in the transient stage to a weaker ENSO in the equilibrium stage. This turnaround of the ENSO amplitude is well consistent with the turnaround of the equatorial thermocline strength, which is also enhanced in the transient stage and in turn reduced in the equilibrium stage. During the entire global warming period, the equatorial atmosphere always stays at a stabler-than-normal state.

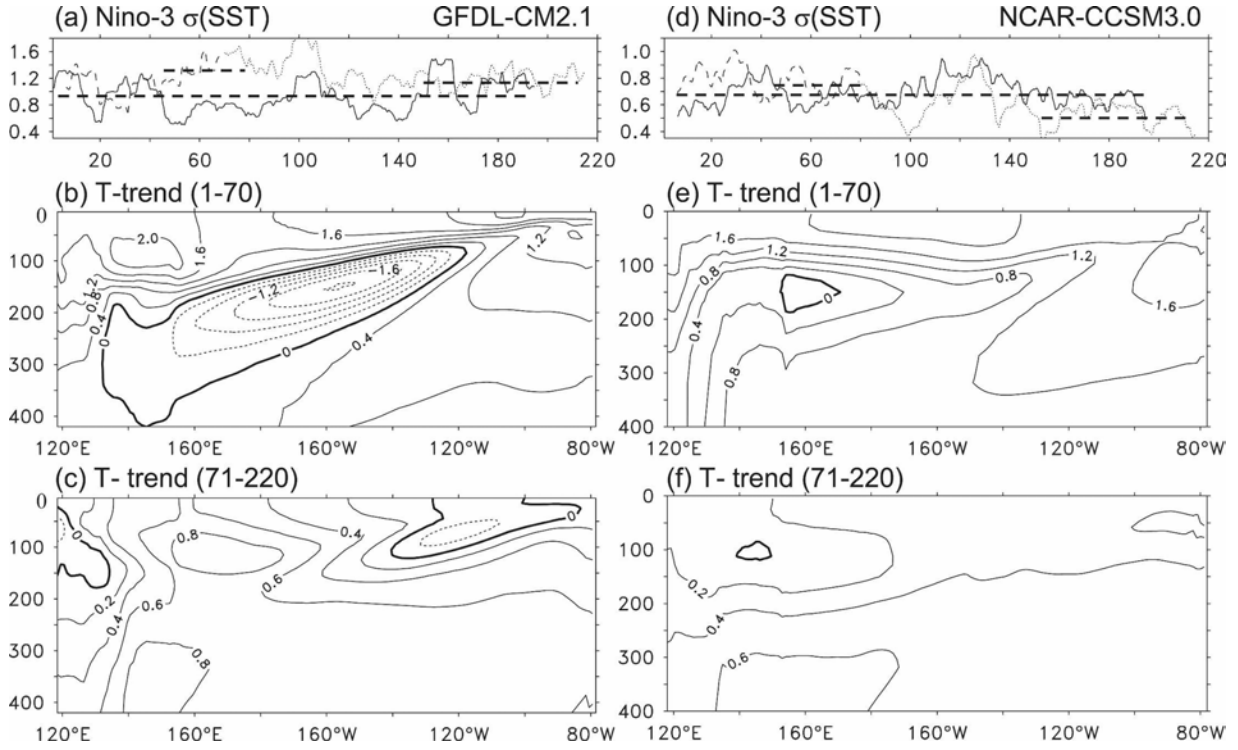

FIG. 14. (a) Time series of SDs (°C) of Niño-3 SST anomaly for control run (solid), "1pctto2x" run over years 1–70 (dashed) and years 71–220 (dotted). Linear trends (°C century^{-1}) of the upper-ocean temperature averaged between 5°S and 5°N over (b) years 1–70 and (c) years 71–220. (left) GFDL CM2.1; (right) NCAR-CCSM3.0. The dashed lines in (a) and (d) represent the mean SDs. For GFDL CM2.1, the values are 0.9°C for control, 1.4°C in years 50–70, and 1.2°C in years 150–220 of 1pctto2x. The corresponding values for NCAR CCSM3.0 are 0.7°, 0.75°, and 0.52°C, respectively. The data are similarly processed as in Fig. 1.

The term balance analyses on the temperature variability equation disclose that the local term, the anomalous upwelling of the mean vertical temperature gradient, dominates the variation of the ENSO variability. The important role of the mean vertical temperature gradient $\overline{T}_z$ in the local term was emphasized in many previous studies (An et al. 2008). In this work, we emphasize that the $\overline{T}_z$ also serves as the background of the $-w'T'$ in the local term. The upward heat flux $-w'T'$ is directly proportional to the $\overline{T}_z$. An increase of $\overline{T}_z$ can cause a bigger increase of $-w'T'$, suggesting that the latter is very sensitive to the former. These two components jointly result in a significant increase of the local term in the 2CO2T. In the 2CO2E, it is also the decrease of $-w'T'$ that results in the decrease of the local term. Therefore, both the direct and indirect dynamic effects of the $\overline{T}_z$ are revealed in this work.

The enhanced ENSO amplitude in the transient stage of future global warming is qualitatively consistent with the observed increasing ENSO variability in the past half century. The discrepancy in the magnitude changes (50% increase in HadISST and only 16% increase in the 2CO2T) may result from the different strength of trends in the mean vertical temperature gradient in the tropics. The estimated $\overline{T}_z$ trend in observation based on Fig. 1b is around 2°–3°C (100m)$^{-1}$ century^{-1} for the tropical upper thermocline, while that in the 2CO2T is about 1°–2°C (100m)$^{-1}$ century^{-1}, much smaller than the observation (figure not shown). This agrees with the argument that stronger equatorial thermocline usually results in a stronger ENSO. The positive relationship between them has been qualitatively investigated in many previous studies, for example, through sensitivity experiments of coupled models (e.g., Meehl et al. 2001) or an intermediate model (e.g., An et al. 2008).

Recently we also checked the ENSO amplitude in two CMIP3/IPCC AR4 models: Geophysical Fluid Dynamics Laboratory Climate Model version 2.1 (GFDL CM2.1) and the National Center for Atmospheric Research's Community Climate System Model, version 3.0 (NCAR CCSM3.0; Zhang et al. 2008). The "20c3m" ensemble experiments from GFDL CM2.1 and 1pctto2x experiments from GFDL CM2.1 and NCAR CCSM3.0 are analyzed. Consistent with our conclusion in this work, these experiments also exhibit the positively proportional relationship between the mean vertical temperature gradient and the ENSO amplitude. In GFDL CM2.1 20c3m, the ENSO amplitude is increased

by about 20% from 1.05°C of 1920–50 to 1.25°C of 1970–2000 (Fig. 13a), in agreement with the enhanced thermocline (Fig. 13b). In GFDL CM2.1 1pctto2x, the ENSO amplitude is first increased by 40% in the transient stage and then reduced by 8% in the equilibrium stage (Fig. 14a), consistent with the enhanced thermocline (Fig. 14b) and weakened thermocline (Fig. 14c), respectively. In NCAR CCSM3.0 1pctto2x, the ENSO amplitude is only increased by 7% in the transient stage but then reduced by 30% in the equilibrium stage (Fig. 14d), also consistent with the enhanced thermocline (Fig. 14e) and weakened thermocline (Fig. 14f), respectively. It is very interesting to notice that the percentage increase in the ENSO amplitude (7% in Fig. 14d, 20% in Fig. 13a, and 40% in Fig. 14a) follows closely with the strength change of the equatorial thermocline (Figs. 14e, 13b, and 14b). This again coincides with the argument that a stronger ENSO is usually related to a stronger equatorial thermocline.

This study emphasizes that the ocean may play a deterministic role in the long-term changes of the ENSO variability. Particularly the subsurface ocean may be more important than expected to the atmosphere–ocean coupled variability. Although this conclusion is also valid in some other coupled models, the mechanisms supporting the conclusions may be different in other models. Moreover, lots of recent studies on some CMIP3 models have also concluded that the global warming has little impact on ENSO (e.g., van Oldenborgh et al. 2005; Merryfield 2006; Guilyardi 2006). The ENSO behaviors and the underlying mechanisms in a warming climate still need to be scrutinized in most coupled models. The observational facts suggest that we should be more prudent on the model results. It might be necessary to reassess the capability of coupled models in modeling the ENSO variability as well as other climate variabilities in a changing world.

Acknowledgments. This work is jointly supported by the NSF of China (No.40576004, 40575044, 40523001) and the National Basic Research Program of China (2007CB411801, 2006CB403602). We thank the international groups for providing observational data and coupled model outputs. The invaluable comments from three anonymous reviewers are greatly appreciated.

APPENDIX

Temperature Variance Equation

Let us start with the temperature equation:

$$\frac{\partial T}{\partial t} = -uT_x - vT_y - wT_y + A_hT_{xx} + A_hT_{yy} + Q_F + R_E. \quad \text{(A1)}$$

Here, $\partial T/\partial t$ is the local temperature tendency; $-uT_x$, $-vT_y$, and $-wT_z$ are the zonal, meridional, and vertical temperature advection, respectively; A_hT_{xx} and A_hT_{yy} are the horizontal diffusion terms with the constant diffusion coefficients A_h (4000 $m^2 s^{-1}$); Q_F is the surface net heat flux forcing (it is zero for the subsurface). The residual term R_E includes the vertical diffusion term and the vertical convection, which is obtained by subtracting the other terms from $\partial T/\partial t$ since it cannot be explicitly calculated.

The temperature in (A1) can be decomposed as $T = \overline{T} + T'$, where the $\overline{T}$ is the mean temperature with climatological seasonal cycle, and T' is the deviation from the mean seasonal cycle. Other variables can be similarly decomposed. The equation for the mean temperature can be written as follows:

$$\frac{\partial \overline{T}}{\partial t} = -\overline{u}\,\overline{T}_x - \overline{v}\overline{T}_y - \overline{w}\,\overline{T}_z + A_h\overline{T}_{xx} + A_h\overline{T}_{yy} + \overline{Q}_F + \overline{R}_E. \quad \text{(A2)}$$

The equation for the temperature anomaly can be obtained by subtracting (A2) from (A1) if we take $\partial\overline{T}/\partial t = 0$ in an equilibrium state:

$$\frac{\partial T'}{\partial t} = -\overline{u}T'_x - u'\overline{T}_x - \overline{v}T'_y - v'\overline{T}_y - \overline{w}T'_z - w'\overline{T}_z + A_hT'_{xx} + A_hT'_{yy} + Q'_F + R'_E. \quad \text{(A3)}$$

Equation (A3) shows that the temperature advection change results from the changes of mean current ($-u'\overline{T}_x$, $-v'\overline{T}_y$, $-w'\overline{T}_z$) and mean temperature gradient ($-\overline{u}T'_x$, $-\overline{v}T'_y$, $-\overline{w}T'_z$). The nonlinear terms ($-u'T'_x$, $-v'T'_y$, $-w'T'_z$) are very small, so they have been neglected in (A3). The temperature gradient here is positive poleward and upward.

Usually the SD of temperature anomaly is calculated as

$$\sigma^2 = \frac{1}{N-1}\sum_{t=1}^{t=N} T'^2(t), \quad \text{(A4)}$$

where the σ is the standard deviation and N is the length of the time series. As far as the temporal evolution of the SD is concerned, (A4) can be rewritten as

$$\sigma^2(t) = \frac{1}{N-1}\sum_{t-N/2}^{t+N/2} T'^2(t). \quad \text{(A5)}$$

Now the N is the width of a sliding window, which can be given in advance. The SD at each time step $\sigma(t)$ is calculated with T' in this window. Thus the local change of $\sigma(t)$ can be derived as

$$\frac{\partial[\sigma^2(t)]}{\partial t} = \frac{1}{N-1}\frac{\partial}{\partial t}\left[\sum_{t-N/2}^{t+N/2} T'^2(t)\right] = \frac{1}{N-1}\sum_{t-N/2}^{t+N/2}\frac{\partial}{\partial t}[T'^2(t)] = \frac{2}{N-1}\sum_{t-N/2}^{t+N/2} T'(t)\frac{\partial T'(t)}{\partial t}. \quad \text{(A6)}$$

Bringing (A3) into (A6), we get

$$\frac{\partial\sigma^2}{\partial t} = \frac{2}{N-1}\sum_{t-N/2}^{t+N/2}\left(\begin{array}{l} -u'T'\overline{T}_x - \overline{u}T'T'_x - v'T'\overline{T}_y - \overline{v}T'T'_y - w'T'\overline{T}_z - \overline{w}T'T'_z \\ +A_hT'T'_{xx} + A_hT'T'_{yy} + T'Q'_F + T'R'_E \end{array}\right); \quad \text{(A7)}$$

(A7) can be referred as temperature variance equation. The terms on the right-hand side provide dynamic connections between physical processes and the amplitude change of temperature. By analyzing these terms, we can explicitly see the mechanisms.

REFERENCES

An, S.-I., J.-S. Kug, Y.-G. Ham, and I.-S. Kang, 2008: Successive modulation of ENSO to the future greenhouse warming. *J. Climate,* **21,** 3–21.

Clarke, A. J., and A. Lebedev, 1996: Long-term changes in the equatorial Pacific trade winds. *J. Climate,* **9,** 1020–1029.

Cobb, K. M., C. D. Charles, H. Cheng, and R. L. Edwards, 2003: The El Niño–Southern Oscillation and tropical Pacific climate during the last millennium. *Nature,* **424,** 271–276.

Cole, J., 2001: A slow dance for El Niño. *Science,* **291,** 1496–1497.

Collins, M., 2000: The El Niño–Southern Oscillation in the second Hadley Centre coupled model and its response to greenhouse warming. *J. Climate,* **13,** 1299–1312.

Fedorov, A. V., and S. G. Philander, 2000: Is El Niño changing? *Science,* **288,** 1997–2002.

——, and ——, 2001: A stability analysis of tropical ocean–atmosphere interaction: Bridging measurements and theory for El Niño. *J. Climate,* **14,** 3086–3101.

Guilyardi, E., 2006: El Niño–mean state–seasonal cycle interactions in a multi-model ensemble. *Climate Dyn.,* **26,** 329–348.

Jacob, R., 1997: Low frequency variability in a simulated atmosphere-ocean system. Ph.D. thesis, University of Wisconsin—Madison, 155 pp.

Liu, Z., and H. Yang, 2003: Extratropical control of tropical climate, the atmospheric bridge and oceanic tunnel. *Geophys. Res. Lett.,* **30,** 1230, doi:10.1029/2002GL016492.

——, J. Kutzbach, and L. Wu, 2000: Modeling climate shift of El Niño variability in the Holocene. *Geophys. Res. Lett.,* **27,** 2265–2268.

Meehl, G. A., P. R. Gent, J. M. Arblaster, B. L. Otto-Bliesner, E. C. Brady, and A. Craig, 2001: Factors that affect the amplitude of El Niño in global coupled climate models. *Climate Dyn.,* **17,** 515–526.

——, H. Teng, and G. Branstator, 2006: Future changes of El Niño in two global coupled climate models. *Climate Dyn.,* **26,** 549–566, doi:10.1007/s00382-005-0098-0.

Merryfield, W. J., 2006: Changes to ENSO under CO_2 doubling in a multimodel ensemble. *J. Climate,* **19,** 4009–4027.

Neelin, J. D., and Coauthors, 1992: Tropical air–sea interactions in general circulation models. *Climate Dyn.,* **7,** 73–104.

Philip, S., and G. J. van Oldenborgh, 2006: Shifts in ENSO coupling processes under global warming. *Geophys. Res. Lett.,* **33,** L11704, doi:10.1029/2006GL026196.

Rayner, N. A., D. E. Parker, E. B. Horton, C. K. Folland, L. V. Alexander, D. P. Rowell, E. C. Kent, and A. Kaplan, 2003: Global analyses of sea surface temperature, sea ice, and night marine air temperature since the late nineteenth century. *J. Geophys. Res.,* **108,** 4407, doi:10.1029/2002JD002670.

Rosenthal, Y., and A. J. Broccoli, 2004: In search of Paleo-ENSO. *Science,* **304,** 219–221.

Stouffer, R. J., and R. T. Wetherald, 2007: Changes of variability in response to increasing greenhouse gases. Part I: Temperature. *J. Climate,* **20,** 5455–5467.

Timmermann, A., M. Latif, A. Bacher, J. Oberhuber, and E. Roeckner, 1999: Increased El Niño frequency in a climate model forced by future greenhouse warming. *Nature,* **398,** 694–696.

Trenberth, K. E., and T. J. Hoar, 1996: The 1990–1995 El Niño–Southern Oscillation event: Longest on record. *Geophys. Res. Lett.,* **23,** 57–60.

Tudhope, A. W., and Coauthors, 2001: Variability in the El Niño–Southern Oscillation through a glacial-interglacial cycle. *Science,* **291,** 1511–1517.

Van Oldenborgh, G. J., S. Y. Philip, and M. Collins, 2005: El Niño in a changing climate: A multi-model study. *Ocean Sci.,* **1,** 81–95.

Vecchi, G. A., and B. J. Soden, 2007: Global warming and the weakening of the tropical circulation. *J. Climate,* **20,** 4316–4340.

——, ——, A. T. Wittenberg, I. M. Held, A. Leetmaa, and M. J. Harrison, 2006: Weakening of tropical Pacific atmospheric circulation due to anthropogenic forcing. *Nature,* **441,** 73–76.

Wu, L., Z. Liu, R. Gallimore, R. Jacob, D. Lee, and Y. Zhong, 2003: Pacific decadal variability: The tropical Pacific mode and the North Pacific mode. *J. Climate,* **16,** 1101–1120.

Yang, H., and Z. Liu, 2005: Tropical–extratropical climate interaction as revealed in idealized coupled climate model experiments. *Climate Dyn.,* **24,** 863–879.

——, H. Jiang, and B. Tan, 2005: Asymmetric impact of the North and South Pacific on the equator in a coupled climate model. *Geophys. Res. Lett.,* **32,** L05604, doi:10.1029/2004GL022195.

Zelle, H., G. J. Van Oldenborgh, G. Burgers, and H. A. Dijkstra, 2005: El Niño and greenhouse warming: Results from ensemble simulations with the NCAR CCSM. *J. Climate,* **18,** 4669–4683.

Zhang, Q., Y. Guan, and H. Yang, 2008: ENSO amplitude change in observation and coupled models. *Adv. Atmos. Sci.,* **25,** 361–366.